

Collisionless Particle Confinement Improvement with the Poloidal-Angle Independent Magnetic Field Components in Helical-Axis Stellarator Configurations

YOKOYAMA Masayuki

National Institute for Fusion Science, Toki 509-5292, Japan

(Received 2 November 1999 / Accepted 12 January 2000)

Abstract

The effects of Radially Increasing Bumpy field (RIB) and the magnetic well (the Radially Increasing Uniform magnetic field (RIU)) on the collisionless particle confinement are examined in helical-axis stellarator configurations. Since these two components do not have the poloidal angle dependence, the radial variation can effectively enhance the poloidal drift with keeping the radial drift unenhanced. The RIB can cause the toroidally-localized closed mod- B_{\min} with the convex radial distribution of the magnetic field strength B around the toroidally-localized minimum of B (B_{\min}) region. On the other hand, the RIU can arise those with concave distribution. When one of them dominates, the improvement of the collisionless particle confinement can be anticipated. This is the case for finite beta cases in W7-X with the magnetic well enhancement. On the contrary, for the Helical-Axis Heliotron (HAH) (such as Heliotron J (H-J)), the radial increase of the bumpy field tends to be enhanced for finite beta cases with simultaneous magnetic well enhancement. This is considered as one reason for the weaker improvement in HAH. An example HAH configuration has been obtained for the RIB to be predominant for a finite beta equilibrium based on the conceptually equivalent coil configuration of H-J. The improvement successfully becomes larger, which implies the usefulness of this systematic study based on the model magnetic field.

Keywords:

helical-axis stellarator configuration, collisionless particle confinement, bumpy field, uniform magnetic field, mod- B_{\min} structure, poloidal drift enhancement

1. Introduction

The Heliotron J (H-J) device [1], based on the Helical-Axis Heliotron (HAH) concept [2,3], has been constructed at the Institute of Advanced Energy, Kyoto University. The experiments have begun from 1999. This concept has arisen to realize the high level compatibility between the good particle confinement and MHD stability with the capability to achieve higher beta value [3]. As for the particle confinement, the bumpy field plays the crucial role to pursue the quasi-isodynamic concept [4] in this configuration, whose

effects have been systematically investigated in Ref. [5].

It is reported that the collisionless particle confinement can be improved for finite beta equilibrium compared to the vacuum case in HAH [2]. The same tendency has been reported also in the W7-X configuration [6] due to the formation of the absolute minimum of B caused by the diamagnetic effect [7]. Comparing these similar results, the improvement has been more significant in W7-X than in HAH.

In this paper, firstly, the reason for the significant improvement in W7-X is considered with clarifying the

author's e-mail: yokoyama@nifs.ac.jp

roles of radially increasing uniform magnetic field. Then, the reason for the weaker improvement in HAH is investigated by comparing the roles of the radially increasing bumpy field and the magnetic well (the radially increasing uniform magnetic field). The aim of this paper is to demonstrate the possibility of further improvement in HAH based on this systematic study.

The model magnetic field is utilized to consider the mod- B_{\min} structure and the magnetic topography, which strongly correlates to particle orbits.

The model magnetic field is described briefly in Sec. 2. The roles of the bumpy field and the uniform magnetic field are explained in Sec. 3 with emphasizing the difference of these two factors. The significant role of the radially increasing bumpy field is briefly described in Sec. 3 for the later comparison. Section 4 is devoted to show an example configuration with the further improvement of collisionless particle confinement in H-J based on this systematic study. Finally, summary is given in Sec. 5.

2. Description of the Model Magnetic Field

The bumpy field typically appears in helical-axis configurations. Therefore, the model magnetic field including the bumpy field is exploited which can be expressed in the Boozer coordinates [8] as

$$B = B_{00}[1 - \epsilon_t \cos \theta_B - \epsilon_h \cos (L\theta_B - M\zeta_B) - \epsilon_b \cos M\zeta_B], \quad (1)$$

where ϵ_t , ϵ_h and ϵ_b denote the toroidicity, helicity and bumpiness, respectively. The $\theta_B(\zeta_B)$ is the poloidal (toroidal) angle, and $L(M)$ the pole number of the

helicity (the number of the field period). In this paper, the toroidicity and helicity with the linear dependence on the plasma minor radius are assumed as frequently the case in helical-axis configurations with the helicity of $L = 1$. The amplitude of the helicity (toroidicity) is fixed as 0.2 (0.1) at the edge, respectively, for simplicity. It is noted that the bumpy field ($L = 0$) is the sideband of the $L = 1$ helicity. For the analysis based on this model magnetic field, $\epsilon_b(0)$ is fixed to be $\epsilon_b(0)/\epsilon_h(a) = -0.5$, which is a relatively good approximation for typical HAH configurations, although its amplitude can be flexibly controlled with coil current combinations. It is noted that this ratio is about -1.2 for the standard W7-X configuration [6] to pursue the quasi-isodynamicity [4]. In this paper, the roles of poloidal-angle independent components, that is, the bumpy field and the uniform magnetic field components for the improvement of collisionless particle confinement in helical-axis stellarator configurations are investigated.

3. The Comparison of Roles of the Bumpy Field and the Uniform Magnetic Field in Collisionless Particle Confinement

3.1 The radial variation of the bumpy field

Figure 1 shows the magnetic field spectra in the Boozer coordinates for (a) vacuum and (b) $\langle\beta\rangle = 2.9\%$ for the configuration considered in Ref. [2]. Here, $\langle\beta\rangle$ denotes the volume averaged beta value. The only four components, uniform magnetic field ($B_{00}(r/a) - B_{00}(0)$ is shown), helicity, toroidicity and bumpiness, are shown for comparison with Eq. (1). The remarkable change of spectra between the vacuum and finite beta equilibria is

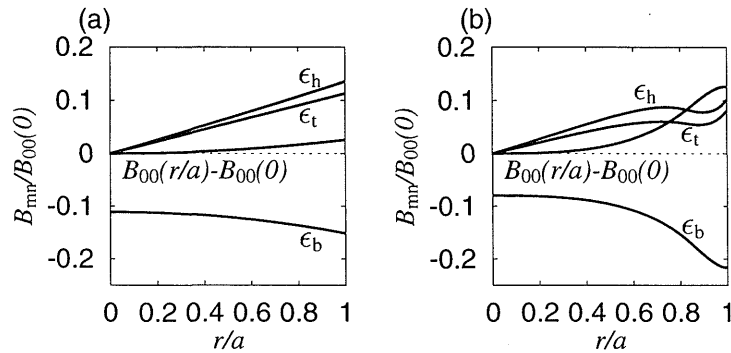


Fig. 1 The magnetic field spectra in the Boozer coordinates for (a) $\langle\beta\rangle = 0.0\%$ and (b) $\langle\beta\rangle = 2.9\%$ for the configuration considered in Ref. [2]. Only the uniform magnetic field ($B_{00}(r/a) - B_{00}(0)$), the main helicity (ϵ_h), the toroidicity (ϵ_t) and the bumpiness (ϵ_b) are shown to compare easily with the model magnetic field.

the increase of the radial variation of the bumpy field and the magnetic well. Since the difference, $B_{00}(r/a) - B_{00}(0)$, is shown in this figure for the uniform magnetic field component, its larger positive slope corresponds to the deeper magnetic well.

First, we briefly mention the role of radially increasing bumpy field for convenience for the later descriptions in this paper. The model bumpy field is

$$\epsilon_b = \epsilon_b(0) [1 + \delta_b(r/a)^2] \quad (2)$$

to model the radial variation of the amplitude. The larger δ_b corresponds to larger increase of the bumpy field towards the plasma edge.

Figure 2 shows the case of (1) $\delta_b = 0$ and (2) $\delta_b = 2$: (a) model magnetic field spectra in the Boozer coordinates, (b) the radial distribution of B on the equatorial plane at the beginning ($\zeta_B = 0$) and the half ($\zeta_B = (1/2)(2\pi/M)$) of the field period, (c) $\text{mod-}B_{\min}$ projected on a poloidal cross section and (d) $\text{mod-}B_{\min}$ projected on the plane with the toroidal direction (one field period) as the horizontal axis and the vertical position as the vertical axis. The minimum value of

$B_{\min}/B_{00}(0)$ is indicated in figure (c). The $B_{\min}/B_{00}(0)$ of the neighboring contour differs 0.025. The figure (d) is to examine the distribution of $\text{mod-}B_{\min}$ along the toroidal direction, which is important to consider in helical-axis configurations where the toroidal localization of B_{\min} region due to the bumpy field can occur. For the case of $\delta_b = 0$, $\text{mod-}B_{\min}$ are toroidally connected (closed) by themselves (see Fig. 2(1)(d)). This is also seen from Fig. 2(1)(b): since B on the equatorial plane at the beginning and the half of the field period has the same minimum value, they expand throughout the full toroidal field period. On the other hand, for the case of $\delta_b = 2$, $\text{mod-}B_{\min}$ are closed with the significantly toroidally-localized B_{\min} region induced by the bumpy field around the half of the field period (see Fig. 2(2)(d)). From Fig. 2(2)(b), it is understood that the magnitude of B between the beginning and the half of the field period is clearly separated. This is effective to localize deeply trapped particles around this region. It is noted that the $\text{mod-}B_{\min}$ are closed with the convex radial distribution of B seen in Fig. 2(2)(b) around the half of the field period.

The property of collisionless particle confinement

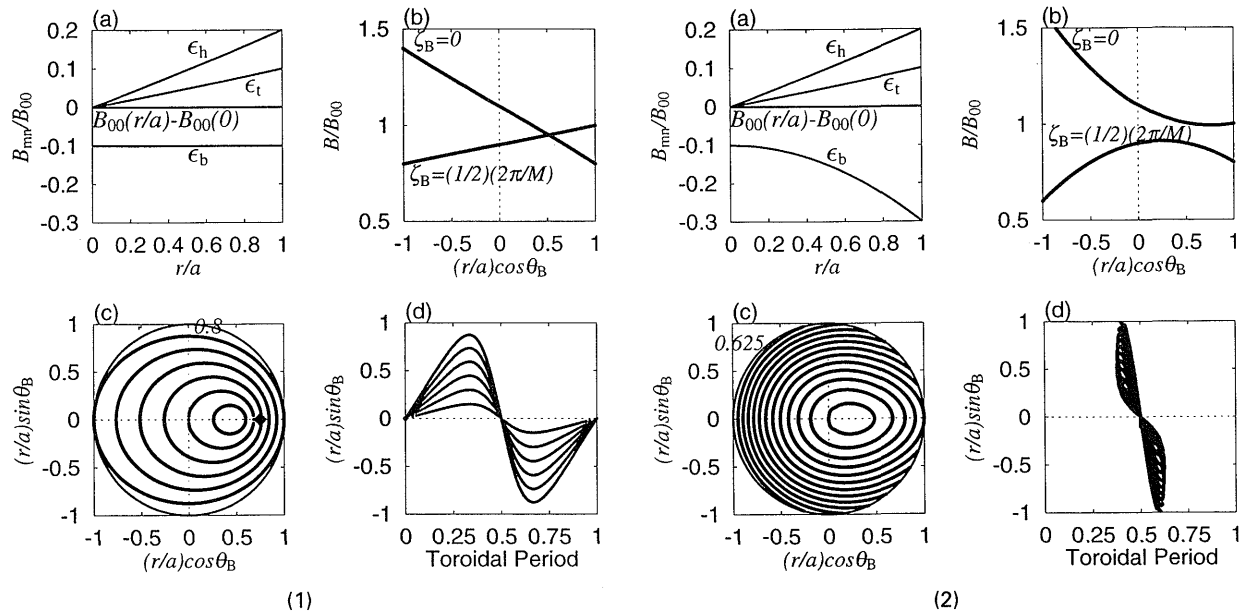


Fig. 2 The case of (1) $\delta_b = 0$ and (2) $\delta_b = 2$: (a) magnetic field spectra in the Boozer coordinates, (b) the radial distribution of the magnetic field strength on the equatorial plane at the beginning ($\zeta_B = 0$) and the half ($\zeta_B = (1/2)(2\pi/M)$) of the field period, (c) $\text{mod-}B_{\min}$ projected on the poloidal cross section and (d) $\text{mod-}B_{\min}$ projected on the plane with the toroidal direction (one field period) as the horizontal axis and the vertical position as the vertical axis. The minimum value of $B_{\min}/B_{00}(0)$ is indicated in Fig. (c). The $B_{\min}/B_{00}(0)$ of the neighboring contour differs 0.025. Figure (d) is valuable to consider the toroidal extension of $\text{mod-}B_{\min}$, which is possible to localize in the toroidal direction with the bumpy field. The $\text{mod-}B_{\min}$ passing $((r/a) \cos \theta_B, \zeta_B) = (0.75, 0)$ is indicated with the diamond for reference in Fig. 2(1)(c).

is compared for different δ_b cases. As δ_b is increased, the collisionless particle confinement is significantly improved [5]. The reason is that the poloidal drift is enhanced through the radial variation of the bumpy field keeping the radial drift unenhanced, which can be understood from the guiding center equations in the Boozer coordinates [9]. For the case with larger δ_b , the region of the enhanced poloidal drift tends to be well aligned to the toroidally-localized B_{\min} region (cf., Fig. 2(2)). This property effectively enhances the poloidal drift for not only deeply trapped particles but also particles launched from outside the B_{\min} region [5], which can make the poloidal closure of drift orbits without transferring to the neighboring toroidal field period. This feature is realized also in the W7-X configuration [7] but based on the different mechanism. The radial variation of the uniform magnetic field plays the crucial role there, which is considered in the next subsection.

3.2 The radial variation of the uniform magnetic field

Now, the reason is considered for the significant improvement of collisionless particle confinement for finite beta equilibria in W7-X. In Ref. [7], the radial distribution of B on the equatorial plane at the beginning and the half of the field period are shown. The clear separation of B is realized even at the vacuum case. As the beta value is increased, the absolute minimum of B

(concave radial distribution) is formed around the half of the field period. It is noted that the magnetic field spectra have little change as beta value is increased in W7-X since the secondary currents are designed to be minimized [6]. Therefore, it is considered that the main difference between the vacuum and finite beta equilibria is the formation of the deeper magnetic well (corresponding to the radially increasing uniform magnetic field) due to the diamagnetic effect. The model uniform magnetic field is considered to imitate such a magnetic well as

$$B_{00} = B_{00}(0) [w + (1 - w)(r/a)^2], \quad (3)$$

where $w = 1$ corresponds to the radially constant uniform magnetic field and $w < 1$ to the magnetic well. The mod- B_{\min} structure for the case of $w = 0.8$ are shown in Fig. 3. The toroidally-localized closed mod- B_{\min} are formed as seen in Fig. 3(c) by the concave radial distribution of B on the equatorial plane around the half of the field period. It is noted that the point-like contour appearing at $(r/a) \cos \theta_B \sim 0.5$ in Fig. 3(c) is the toroidally connected mod- B_{\min} (cf., Fig. 3(d)) as a result from the same B at the beginning and the half of the field period as seen in Fig. 3(b).

The effect of the radially increasing uniform magnetic field on collisionless particle confinement is considered here. Three cases with $\delta_b = 0$ (radially constant bumpy field) and different values of w are considered. Proton motions are calculated based on the guiding center equations in the Boozer coordinates for the average B of 1 T on the magnetic axis. They are launched from magnetic surfaces with $r/a = 1/4, 1/2$ and $3/4$ with a uniform distribution in the pitch angle in velocity space (15 points). The launching points are uniformly distributed in the poloidal (10 points) and toroidal (10 points) angles on each magnetic surface. The number of launched particles from each point is determined by considering the variation of the area element, $dS = J |\nabla \psi| d\theta_B d\zeta_B$ on a magnetic surface. Here, J denotes the Jacobian of the Boozer coordinates. The total number of followed protons is 6105 for each case. The particle is defined to be lost when it crosses the plasma boundary. The proton temperature profile is assumed as $T_i = 1.0[1 - (r/a)^2]$ keV. This profile gives the proton energy of 0.9375, 0.75 and 0.4375 keV at the above three radii, respectively. As for reference, 1 keV proton has $\rho_l/a \sim 2.4 \times 10^{-2}$, where ρ_l is the Larmor radius. This ratio corresponds to that of 70 keV proton in W7-X. They are followed for 2 ms. The selection of

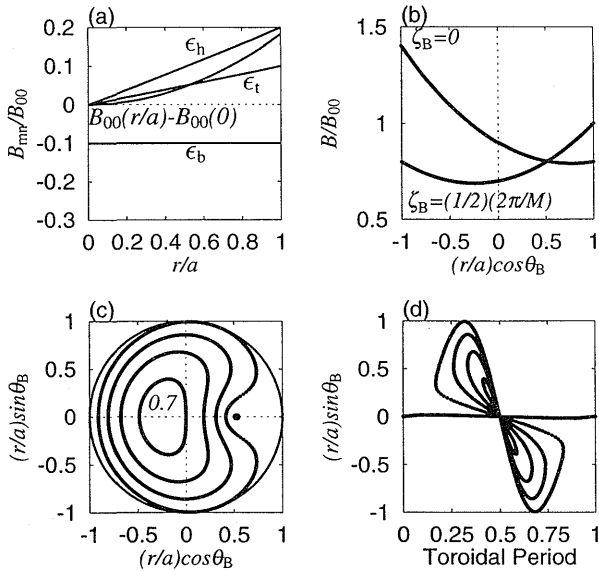


Fig. 3 The mod- B_{\min} structure for the case of $w = 0.8$.

the following time, 2 ms, is based on the ion-ion collision time (about 2.2 ms for $T_i \sim 1$ keV and the density of about 10^{19} m^{-3}), which is an example parameter to examine the behavior of prompt loss. The longer following time should be required, of course, for the case with longer collision time.

The time traces of loss rate for these three cases are shown in Fig. 4. The trapped particle rate (of 6105 particles) is about 25% for each case. For $w = 1.0$ and 0.9 cases, where toroidal localization of closed mod- B_{\min} is not remarkable, trapped particles launched from the

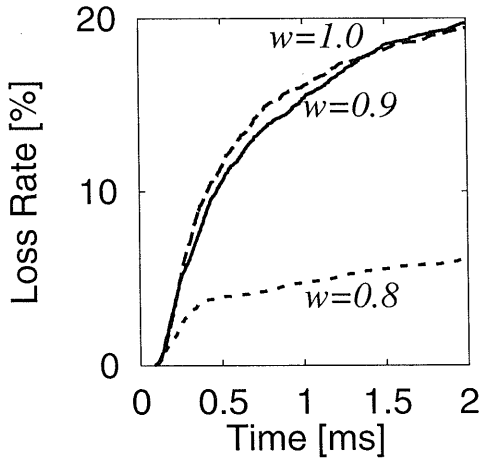


Fig. 4 The time trace of particle loss rate for the cases of $w = 1.0, 0.9$ and 0.8 .

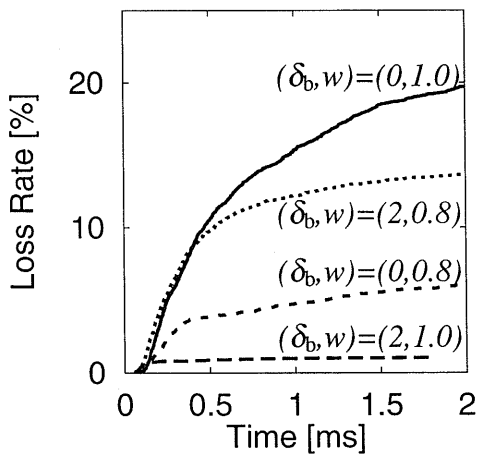


Fig. 5 The time trace of particle loss rate for the cases with different combination of (δ_b, w) . The $\delta_b > 0$ denotes the radially increasing bumpy field and $w < 1$ the magnetic well.

region where mod- B_{\min} do not exist are quickly lost due to the radial drift. For example, the mod- B_{\min} marked with the diamond in Fig. 2(1)(c) passes $((r/a) \cos \theta_B, \zeta_B) = (0.75, 0)$ and there are no mod- B_{\min} around $\zeta_B \neq 0$ on $(r/a) \cos \theta_B = 0.75$. Trapped particles launched from this region ($\zeta_B \neq 0$) are easily lost, and totally, about 80% of trapped particles (20% of total particles) are lost within 2 ms. On the other hand, the toroidally-localized closed mod- B_{\min} with absolute minimum of B are remarkably realized as in Fig. 3(c) and (d). In this case, when trapped particles reach the region of the absolute minimum of B (around the half of the field period) before escaping, their poloidal drift is rather enhanced with the radially increasing uniform magnetic field, which results in the reduction of loss rate within 2 ms. This is the case for particles launched from $r/a = 1/4$, where the absolute minimum of B extends throughout the poloidal direction (cf., Fig. 3(c)). Therefore, the effective reduction is seen for particles launched from $r/a = 1/4$. For reference, the loss rates are 15.1%, 18.8% and 20.4% for particles launched from $r/a = 1/4, 1/2$ and $3/4$ for $w = 1.0$ case, and these values decrease to 0.2%, 6.1% and 8.3%, respectively, for $w = 0.8$ case.

3.3 Radially increasing bumpy field and simultaneous radially increasing uniform magnetic field

The toroidally-localized closed mod- B_{\min} are formed with the convex radial distribution for the radially increasing bumpy field (cf., Sec. 3.1) and with the concave radial distribution for the radially increasing uniform magnetic field (cf., Sec. 3.2), both which can effectively enhance the poloidal drift when they occur individually. Here, it is considered the case where these two effects occur simultaneously. The collisionless particle loss rates are shown in Fig. 5. The $(\delta_b, w) = (0, 1.0)$ corresponds to the case with the radially constant bumpy field without the magnetic well. The $(\delta_b, w) = (2, 1.0)$ to the radially increasing bumpy field without the magnetic well, $(\delta_b, w) = (0, 0.8)$ to the radially constant bumpy field with the magnetic well (cf., $w = 0.8$ case shown in Fig. 4) and $(\delta_b, w) = (2, 0.8)$ to the radially increasing bumpy field with the simultaneous magnetic well, respectively.

It is seen that each effect effectively improves the collisionless particle confinement through the enhancement of the poloidal drift. The lost particles have a wide range of initial launching position in the toroidal direction ($0 \leq \zeta_B / (2\pi/M) \leq 1$) for the case of $(\delta_b, w) = (0, 1.0)$ with the initial pitch angle of $60^\circ \leq \lambda \leq$

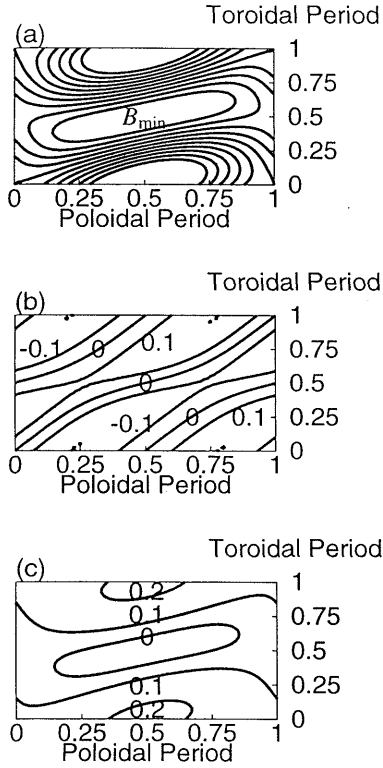


Fig. 6 The topography for (a) B , (b) $(1/B)(\partial B/\partial\theta_B)$ and (c) $(\psi/B)(\partial B/\partial\psi)$ at $r/a = 0.75$ for the case of $(\delta_b, w) = (2, 0.8)$. In Fig. (b), the radial drift is cancelled out on the contour with 0, and outward (inward) with positive (negative) value, and in Fig. (c), the poloidal drift is enhanced in the region with larger value, for example, 0.2.

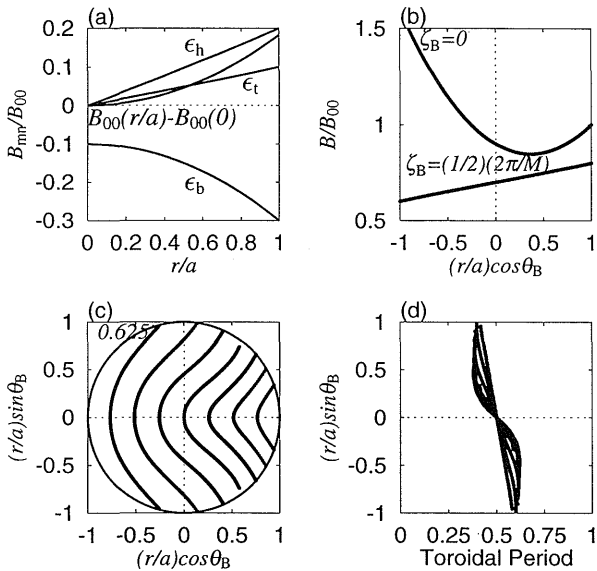


Fig. 7 The mod- B_{\min} structure for the case of $(\delta_b, w) = (2, 0.8)$.

120°, where $\lambda \equiv \arccos(v_{\parallel}/v)$ with v_{\parallel} and v the velocity parallel to the magnetic field and the total velocity. The escaping points are distributed throughout the toroidal field period due to the independence of the uniform magnetic field on the toroidal angle. On the other hand, for the case of $(\delta_b, w) = (2, 1.0)$, all particles launched from $r/a = 1/4$ and $1/2$ are confined within 2 ms, while 2.5% from $r/a = 3/4$ are lost. These lost particles are launched from $0.25 \lesssim \zeta_B/(2\pi/M) \lesssim 0.75$ with $\lambda \sim 90^\circ$. Since the poloidal drift enhancement through the radial variation of B requires the parallel velocity [9], this effect is weak for particles with $\lambda \sim 90^\circ$. The escaping points of lost particles is also localized around the half of the field period, which implies that these lost particles are deeply trapped in the bumpy field ripple with rather small parallel velocity. As for the case of $(\delta_b, w) = (0, 0.8)$, the loss rate reduction is remarkable for $r/a = 1/4$ as mentioned in Sec. 3.2 with the formation of the absolute minimum of B . The particles launched from around the half of the field period with the initial pitch angle of $\lambda \sim 90^\circ$ becomes confined within 2 ms even launched for $r/a = 1/2$ and $3/4$, which contributes to the loss rate reduction for these radii. It should be noted that the escaping points are distributed throughout the toroidal field period as for the case of $(\delta_b, w) = (0, 1.0)$.

When these two effects occur simultaneously, $(\delta_b, w) = (2, 0.8)$, the improvement becomes weaker. Its reason is considered to be the suppression of poloidal drift because the radial variation of B around the B_{\min} region tends to be cancelled out with the opposing convex and concave distribution due to these two effects. The topography of (a) B , (b) $(1/B)(\partial B/\partial\theta_B)$ and (c) $(\psi/B)(\partial B/\partial\psi)$ at $r/a = 0.75$ are shown in Fig. 6. The $(1/B)(\partial B/\partial\theta_B)[(\psi/B)(\partial B/\partial\psi)]$ is considered as a convenient measure for the radial [poloidal] drift [9]. In Fig. 6(b), the radial drift is cancelled out on the contour with 0, and outward (inward) with positive (negative) value. On the other hand, in Fig. 6(c), the poloidal drift is enhanced in the region with larger number, for example, 0.2. There is no qualitative difference for $(1/B)(\partial B/\partial\theta_B)$ compared to the case of $(\delta_b, w) = (2, 1.0)$ [5]. The significant difference is that the region of enhanced poloidal drift deviates from the B_{\min} region for this case. The mod- B_{\min} structure is shown in Fig. 7. It is noted that the time trace of loss rate does not depend much on initial launching radii for this case, which is understood from the distribution of mod- B_{\min} throughout the plasma shown in Figs. 7(c) and (d) (open, similar shape with similar toroidal extension). The escaping points in the toroidal direction are distributed around

$0.25 \leq \zeta_B/(2\pi/M) \leq 0.75$, whose extension is considered to be intermediate between the case of $(\delta_b, w) = (2, 1.0)$ and $(0, 0.8)$.

4. The Possibility of Further Improvement of Collisionless Particle Confinement in Heliotron J

Based on the systematic understandings with the model magnetic field, one example configuration possible with the real coil configuration is considered for further improvement in H-J. Here, the magnetic field spectra for finite beta case shown in Fig. 1(b) is reconsidered. It is seen that the radial increase of the bumpy field is enhanced with the simultaneous diamagnetic effect. This situation corresponds to that described in Sec. 3.3. The mod- B_{min} structure for the case of $\langle\beta\rangle = 2.9\%$ considered in Ref. [2] is shown in Fig. 8. To simplify the comparison with the above described model magnetic field, only the four spectra, the uniform, main helicity, toroidicity and the bumpiness, are taken into account (cf., Fig. 8(a)), although several other components also exist. The toroidally-localized closed mod- B_{min} are formed seen in Fig. 8(d). However, as in Fig. 8(b), B on the equatorial plane around the half of the field period is almost radially constant. It is considered that the convex radial variation formed by the radially increasing bumpy field is cancelled with the concave variation due to the diamagnetic effect. Figure 9 shows the topography of (a)

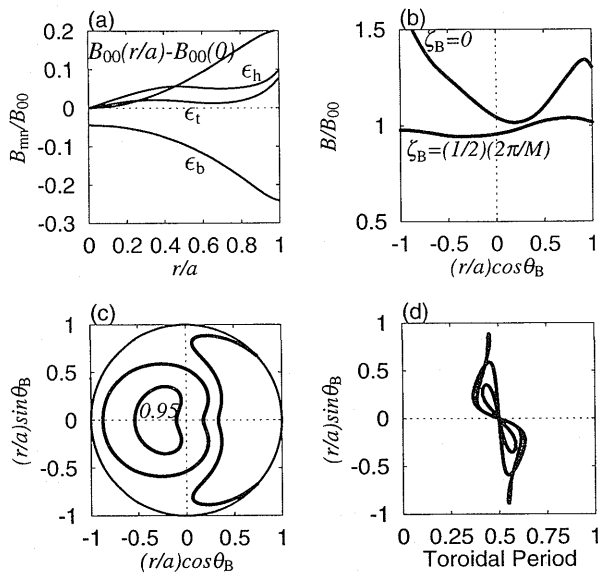


Fig. 8 The mod- B_{min} structure for the configuration with $\langle\beta\rangle = 2.9\%$ considered in Ref. [2].

B , (b) $(1/B)(\partial B/\partial\theta_B)$ and (c) $(\psi/B)(\partial B/\partial\psi)$ at $r/a = 0.75$. These figures are qualitatively equivalent to those obtained for the model magnetic field with $(\delta_b, w) = (2, 0.8)$ shown in Fig. 6, although the values and distribution are different reflecting the real magnetic field spectra in Fig. 8(a). This equivalence indicates that the considerations in Sec. 3.3 based on the model magnetic field are applicable to this configuration. It is seen in Fig. 9(c) that the region of the enhanced poloidal drift deviates from the B_{min} region. It is concluded that one of the reasons for the weaker improvement of collisionless particle confinement for finite beta cases compared to the vacuum case in H-J than W7-X is that the enhancement of the poloidal drift is weakened by the radially increasing bumpy field with the simultaneous diamagnetic effect.

The following four ideas can be considered to maintain the enhancement of the poloidal drift due to the one of these two effects:

- i. the stronger radially increasing bumpy field at vacuum case to overcome the diamagnetic effect for finite beta case,

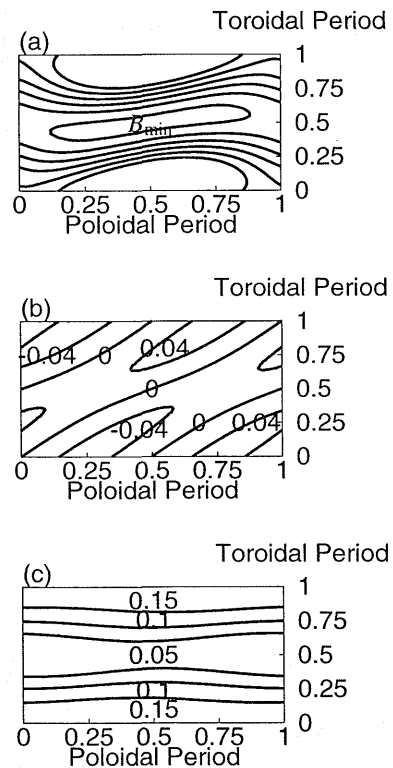


Fig. 9 The topography for (a) B , (b) $(1/B)(\partial B/\partial\theta_B)$ and (c) $(\psi/B)(\partial B/\partial\psi)$ at $r/a = 0.75$ for the configuration shown in Fig. 8.

- ii. contrary to (i), the radially decreasing bumpy field at vacuum case for the diamagnetic effect to be predominant for finite beta case,
- iii. the deeper vacuum magnetic well to maintain the predominance of the diamagnetic effect for finite beta case,
- iv. contrary to (iii), the vacuum magnetic hill to make the diamagnetic effect induced magnetic well shallower for the role of the bumpy field to be predominant.

The item (iv) is inadequate from the viewpoint of the compatibility with MHD stability. The idea (ii) also may not be suitable since the vacuum magnetic well formation has been rather difficult for the configuration with the radially decreasing bumpy field. Here, one example configuration is shown, which has been obtained based on the idea (i) with the coil configuration conceptually equivalent to that of H-J. The configuration can be realized with increasing the coil current in the Inner Vertical (IV) coils with the current direction same as in helical coil. The IV coils are located not far from the geometrical equatorial plane (the height is ± 0.17 m for H-J) with the smaller major radius (0.425 m) than the plasma (about 1.2 m). When the helical coil passes the innerside of a torus, B is enhanced because the currents in helical and IV coils locate at the same side of the plasma. On the other hand, when the helical coil passes the outside of a torus, the helical coil and IV

coils locate at the opposite side of the plasma, which weakens B . This variation of B along the toroidal direction can amplify the bumpy field. Figure 10(1) shows the vacuum case with only four field components taken into account. It is seen from Fig. 10(1)(a) that the bumpy field has substantial radial increase, which corresponds already to $\delta_b \sim 2$. It is noted that the toroidicity is also enhanced, which may result in the larger Pfirsch-Schlüter current to degrade the equilibrium beta limit. As shown in Fig. 10(1)(b), B on the equatorial plane is almost separated between the beginning and the half of the field period. The mod- B_{\min} are not closed except the core region, although they are toroidally localized around the half of the field period with the convex radial distribution of B . The case of $\langle \beta \rangle = 1.3\%$ is shown in Fig. 10(2), where the radial increase of the bumpy field overcomes the diamagnetic effect, which keeps the convex radial distribution of B . The separation of B between the beginning and the half of the field period is successfully realized, which localizes the region where trapped particles exist and also enhances the formation of the toroidally-localized closed mod- B_{\min} . The collisionless particle loss rate is shown in Fig. 11, which indicates the successful reduction of the loss rate for finite beta equilibrium at least until 2 ms. The increment of loss rate also reduces, which has not been demonstrated as shown in Ref. [2].

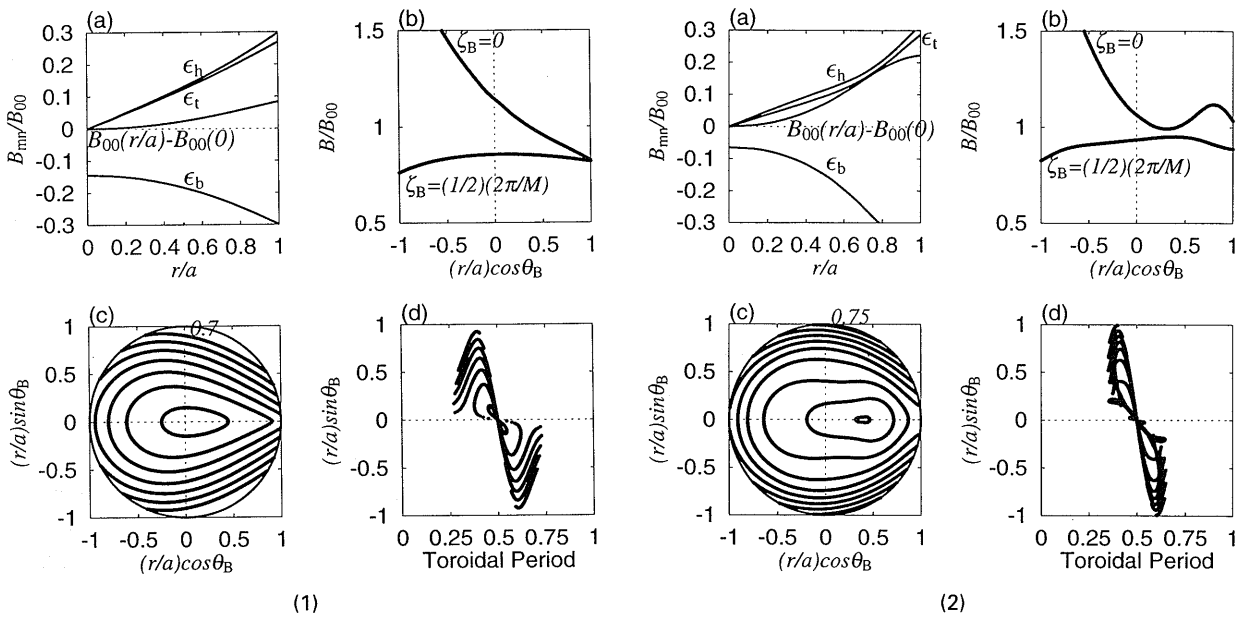


Fig. 10 The case for the configuration obtained with increasing the coil current in the inner vertical coils based on the coil configuration conceptually equivalent to that of H-J: (1) $\langle \beta \rangle = 0.0\%$ and (2) $\langle \beta \rangle = 1.3\%$.

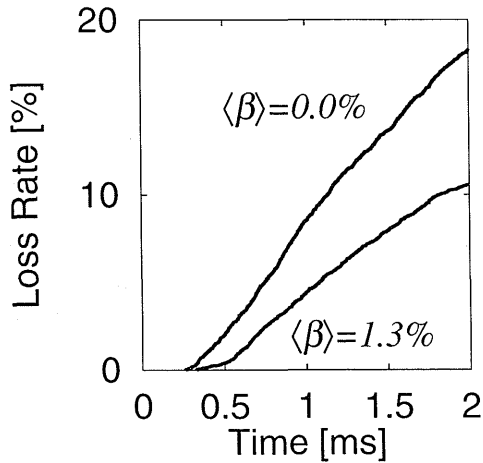


Fig. 11 The time trace of particle loss rate for the configuration shown in Fig. 10.

This may be the result of the successful formation of the toroidally-localized mod- B_{\min} with the poloidal drift enhancement due to the large radial increase of the bumpy field. Of course, the longer following calculation is required for cases with longer ion-ion collision time since the loss rate still increases at 2 ms. However, it is the aim here to demonstrate the possibility of improvement of collisionless particle confinement in H-J and this result is promising. The improvement for finite beta equilibria is also enhanced compared to a few percent for the previous case [2]. Since particle orbits are followed with 30 field components there [2], the decrease of the loss rate for this configuration can not be considered only due to the enhancement of the radial increase of the bumpy field. However, it is anticipated that the radial increase of the bumpy field plays the significant role for this improvement based on the systematic investigations in this paper based on the model magnetic field.

5. Summary

The improvement of collisionless particle confinement has been considered systematically based on the model magnetic field, taken W7-X and Heliotron J (H-J) as examples.

The role of the radially increasing bumpy field is investigated, which is typically the case for finite beta equilibria in H-J. The following characteristics are given by this bumpy field:

- toroidally-localized B_{\min} region,
- the bumpy field has no poloidal angle dependence, which does not affect the radial

drift even if its amplitude is enhanced,

- the radial variation (here the increase) enhances the poloidal drift.

The region with larger poloidal drift is well aligned to the region of the local minimum of B with keeping the radial drift unenhanced. In this case, toroidally-localized closed mod- B_{\min} are formed with the convex radial distribution of B on the equatorial plane around the half of the field period.

On the other hand, the diamagnetic effect is also considered to be the reason for the significant improvement of collisionless particle confinement for finite beta equilibria in W7-X. The magnetic well enhancement (that is the radial increase of the uniform magnetic field component) by the diamagnetic effect for finite beta equilibria is only one significant difference in the magnetic field spectra between vacuum and finite beta cases. Also in this case, the toroidally-localized closed mod- B_{\min} are formed. The uniform magnetic field also does not have the poloidal angle dependence, whose radial variation can enhance the poloidal drift without enhancing the radial drift. The reason for improvement in W7-X is this poloidal drift enhancement due to the diamagnetic effect for finite beta equilibria. It is noted that the toroidally-localized closed mod- B_{\min} are formed with the concave radial distribution of B on the equatorial plane around the half of the field period. This is opposite to that caused by the radially increasing bumpy field.

The radially increasing bumpy field and the diamagnetic effect occur simultaneously for typical finite beta equilibria in H-J. Although the toroidally-localized mod- B_{\min} can be formed, the radial variation of the field strength around this region tends to be weakened with these simultaneous two effects. This is considered as one reason for the weaker improvement in H-J than that in W7-X.

The several ideas can be considered to prevent this unfavorable fact. The one of those ideas is realized with the coil configuration conceptually equivalent to that of H-J. This example configuration, which has a stronger radial increase of the bumpy field even at the vacuum case, is possible with the increase of the coil current in the IV coils. This radial variation is enough to form the toroidally-localized mod- B_{\min} with the convex radial distribution of B on the equatorial plane around the half of the field period, where local minimum of B locates. The effect of the radially increasing bumpy field overcomes the effect of the diamagnetic effect, which successfully improves the collisionless particle

confinement for finite beta equilibrium.

The further improvement and experimental test should be pursued with the real coil configuration based on this systematic study. As described in Sec. 3, escaping points of lost particles are relatively localized around the half of the field period as the radial variation of the bumpy field is enhanced. On the other hand, they spread throughout the toroidal field period for a case of radially increasing uniform magnetic field due to its independence on the toroidal angle. Therefore, measurements for the toroidal distribution of lost particles can give the information which is dominant between the bumpy and uniform magnetic field to form the toroidally-localized mod- B_{\min} .

Acknowledgements

The author gratefully acknowledges productive and fruitful discussions with Prof. M. Wakatani and Dr. S. Murakami. The precious comments from Prof. J. Todoroki to let the author notice the possibility of the toroidally-localized mod- B_{\min} are also appreciated. The careful reading and precious comments by referees are valuable to improve this paper. This work has been

supported by grant-in-aid from the Ministry of Education, Science, Sport and Culture (Monbusho), Japan.

References

- [1] F. Sano *et al.*, *J. Plasma Fusion Res.* **75**, 222 (1999).
- [2] M. Yokoyama, Y. Nakamura and M. Wakatani, *Proc. 16th IAEA Fusion Energy Conf.* 1996, IAEA, Vienna (1997) Vol. 2, p.175.
- [3] M. Wakatani *et al.*, *Proc. 17th IAEA Fusion Energy Conf.* (1998) IAEA-CN-69/ICP/08(R).
- [4] S. Gori, W. Lotz and J. Nührenberg, *Theory of Fusion Plasmas (Proc. Workshop Varenna, 1996)* Editrice Compositori, Bologna (1997) p.335.
- [5] M. Yokoyama *et al.*, *to appear in Nucl. Fusion* **2** (2000).
- [6] G. Grieger *et al.*, *Phys. Fluids B* **4**, 2081 (1992).
- [7] W. Lotz *et al.*, *Plasma Phys. Control. Fusion* **34**, 1037 (1992).
- [8] A. Boozer, *Phys. Fluids* **23**, 904 (1980).
- [9] R.H. Fowler *et al.*, *Phys. Fluids* **28**, 338 (1985).